Edge-On (Cellulose II) and Face-On (Cellulose I) Adsorption of Cellulose Nanocrystals at the Oil–Water Interface: A Combined Entropic and Enthalpic Process

Somia Haouache, Yu Chen, Clara Jiménez-Saelices, Fabrice Cousin, Pan Chen, Yoshiharu Nishiyama, François Jerome, Isabelle Capron

HAL Id: hal-04185901
https://hal.inrae.fr/hal-04185901

Submitted on 23 Aug 2023

Edge-on (cellulose II) and face-on (cellulose I) adsorption of cellulose nanocrystals at the oil/water interface; a combined entropic and enthalpic process.

Somia Haouache[1,2,#], Yu Chen[3,#], Clara Jimenez-Saelices[1], Fabrice Cousin[4], Pan Chen[3], Yoshiharu Nishiyama[5], François Jerome[2], Isabelle Capron[1]

1- INRAE, UR BIA, F-44316, Nantes, France

2- ICMMP, Université de Poitiers-CNRS, Poitiers, France

3- Beijing Engineering Research Centre of Cellulose and Its Derivatives, School of Materials Science and Engineering, Beijing Institute of Technology, 100081, Beijing, P.R. China

4- Laboratoire Léon Brillouin, Université Paris-Saclay, CEA-CNRS, CEA-Saclay, Gif-sur-Yvette, France

5- CERMAV, University Grenoble Alpes, CNRS, F-38000 Grenoble, France.

# contributed equally

Abstract

Nanocelluloses can be used to stabilize oil/water surfaces, forming so-called Pickering emulsions. In this work, we compare the organization of native and mercerized cellulose nanocrystals (CNC-I and CNC-II) adsorbed on the surface of hexadecane droplets dispersed in water at different CNC

concentrations. Both types of CNC have an elongated particle morphology and form a layer strongly adsorbed at the interface. However, while the layer thickness formed with CNC-I is independent of the concentration at 7 nm, CNC-II forms a layer ranging from 9 to 14 nm thick with increasing concentration, as determined using small angle neutron scattering with contrast matched experiments. Molecular dynamics (MD) simulations showed a preferred interacting crystallographic plane for both crystalline allomorphs that exposes the CH groups (1 0 0 and 0 1 0) and is therefore considered hydrophobic. Furthermore, this study suggests that whatever the allomorph, the migration of CNCs to the oil-water interface is spontaneous and irreversible, and is driven by both enthalpic and entropic processes.

INTRODUCTION

Cellulose is an abundant natural renewable resource that accounts for more than half of the earth's biomass. It is being developed for a wide variety of applications due to unique combination of sustainability, scalability, low density, chemical and mechanical stabilities. Cellulose is produced in nature as slender crystalline microfibrils with small width, ranging between 2-20 nm depending on the biological origin,[1] and more specifically on the arrangement of the synthesis complex at the synthesizing loci. The crystallization at the vicinity of polymerizing loci leads to the well-defined lateral size and almost infinite length of the microfibrils. In most organisms the microfibrils are wrapped with hemicellulose, heteropolysaccharides with high affinity to the cellulose surface,[2] that can be easily removed by chemical treatments. Such naked microfibrils might collapse to each other, especially when dried, leading to local aggregation with neighboring fibrils. For higher plant cellulose, hydrolysis of such aggregated structure leads to particles of relatively uniform length, called "cellulose nanocrystals" (CNC) that are often lateral aggregate of elementary crystallites.[3]

2

Cellulose chains show almost orthotropic characters with three orthogonal directions with distinct characteristics: i) the chain direction where residues are linked through covalent bonds, ii) the equatorial direction which is the direction in the plane of the pyranose perpendicular to the chain axis where the three hydroxyl groups are located, and iii) the axial direction dominated by CH groups.[4] The axial surface is less exposed than the other two surfaces when the crystallization process occurs in an aqueous environment, which is the case of native cellulose (cellulose I). When cellulose is swollen in concentrated alkali solution, typically above 4N NaOH at room temperature, the alkali penetrates crystalline region leading to high degree of swelling, and recrystallizes into mercerized cellulose (cellulose II) when washed with water, thus again in aqueous environment.[5] Still this surface often plays an important role, for example in anchoring cellulose binding domains of cellulases.[6] This surface might be also contributing to the ability of CNC to stabilize oil-water interface.

Oza and Frank reported first in 1989, that microcrystalline cellulose can replace conventional surfactants in oil-in-water emulsions.[7] Despite being considered hydrophilic, nanocelluloses adsorb efficiently at oil-water interfaces to produce highly stable emulsions armored by a layer of solid particles, which are called Pickering emulsions.[8, 9] In order to depict the mechanisms that drive the formation of emulsions, adsorption of the crystalline part has been deeply investigated since 2011.[10-12] These emulsions, stabilized by unmodified CNC at very low concentration (below 0.1wt%), are stable for months due to an irreversible adsorption of CNC at the oil interface. This behavior has triggered a strong interest in the cellulose and colloids communities.[13, 14] In previous studies, we assumed that the nanorods of native cellulose strongly adsorb to the oil phase along the longest axis, most probably via the less polar (1 0 0) crystalline plane surface [11, 12, 15] bending along the surface down to average drop diameters as small as 350 nm.[16] This was however still not fully validated. The interfacial properties of nanoparticles are generally correlated to their surface chemistry and organization, but the way how CNCs interact with the oil surface is still not fully understood.[17] [18] [19] A strategy to go further in the description of the mechanism is to compare the behavior of different cellulose types at such interfaces and notably compare cellulose-I type to mercerized cellulose (cellulose-II type) with a different crystalline exposed planes and antiparallel chains. Li *et al*. reported that CNC-II had lower ability to

stabilize oil-in-water emulsions than CNC-I, but the size of the CNC-II they used was much smaller than the CNC-I under scrutiny, making the comparison complicated.[19]

We apply the same approach here, where we investigate the affinity of two CNC allomorphs that have very close structural features, to the oil-water interface, and their ability to stabilize the Pickering emulsions to try to obtain more molecular insights at the interface. The allomorphs were obtained from native fibers and characterized in a recent study.[20] Briefly, the native fibers (MFC-I) were converted into mercerized MFC-II form without any molar mass variation of individual chains, i.e. without any degradation of the cellulose chains. Once the fibers hydrolyzed with sulfuric acid, CNC-I and CNC-II showed identical surface charge density, but the CNC-II recovered were shorter in length and with smaller particle molar masses as well as molar masses of dissolved individual cellulosic chains.[20,21] The lateral dimension of CNC-II was similar to that of CNC-I but the thickness was about half that of CNC-I.

EXPERIMENTAL SECTION

Materials

Native cotton cellulose fibers (MFC) were obtained from Whatman filters (grade 20). All reagents were acquired from Sigma Aldrich and used without further purification. Water was purified with a Milli-Q system (18.2 MΩ cm Millipore Milli-Q purification system).

Cellulose samples preparation

Native cotton cellulose fiber (MFC-I) was mercerized into MFC-II according to a protocol similar to that described by Neto et al.[18] In short 10 g of MFC-I was introduced into 300 mL of 20% aqueous NaOH solution and mechanically stirred for 5 h at 25°C. The mixture was washed several times with distilled water in order to remove the NaOH, and then dried at 40°C for 48h. The yield of this conversion process was 100%.

Cellulose nanocrystals (CNC-I and CNC-II): The cellulose nanocrystals were then prepared using the same hydrolysis with sulfuric acid according to the method of Revol et al. with minor modifications.[22] Briefly, MFC-I and MFC-II were hydrolyzed using 64% sulfuric acid at 68°C under stirring for 20 min. After hydrolysis, the suspension was washed by centrifugation, dialyzed to neutrality against Milli-Q water for 2 weeks, and deionized using mixed bed resin (TMD-8) to remove all residual sodium ions. The final dispersion was sonicated for 10 min, filtered, and stored at 4 °C. The yield was 64% and 40% for CNC-I and CNC-II respectively. The suspensions prepared at various concentrations were systematically sonicated using intermittent pulses with an ultrasonic device with a dipping titanium probe for 4 min at sonication amplitude 50. Samples characterization including surface charge performed by conductometric titration with a 0.001 M NaOH and zeta potential as well as average dimensions of the crystals determined from SANS, TEM and AFM image analysis are in reference[23] and are recapitulated here in Table 1.

Emulsions Preparation and characterization

The hexadecane-in-water Pickering emulsions were prepared by mixing an aqueous dispersion of CNC at various concentrations (g/L), with hexadecane at a 20/80 O/W volume fraction. The concentration was after that defined in g of CNC / mL of hexadecane (m_p) that is the relevant parameter to get rid of the oil/water ratio and characterize the emulsion. For all the emulsions, the oil phase was hexadecane and the aqueous phase was CNC-I or CNC-II aqueous suspensions. The suspensions were diluted at different concentrations with a 50 mM NaCl aqueous solution. This ionic strength was chosen as it allows to screen electrostatic repulsions due to sulfate groups present at the surface of CNCs without promoting strong CNC aggregation,[24, 25] Such a salinity was successfully used in previous papers to design emulsions[11, 12] because: (i) it avoids the situation where a first adsorbed CNC at the O/W interface prevents the adsorption of a next one in its vicinity; (ii) the weak aggregates obtained are easily broken upon sonication during emulsion formation. In order to compare how the CNC types behave in suspension, we studied their aggregation behavior as a function of salinity by SANS (see Figure SI.1), as done in previous studies.[24] CNC-I behaves exactly as in former studies with formation of aggregates of a few nanocrystals at 50mM. Moreover, CNC-II shows exactly

the same behavior (see table 1). Emulsions were sonicated for 60 s using intermittent pulses (1 on / 2 off) with an ultrasonic device with a dipping titanium probe close to the surface placed in ice. The sonication amplitude corresponds to 4 W/mL.

This protocol allows the full adsorption of the CNCs at the interface as demonstrated in two previous studies. In a first study, the residual CNC content in the aqueous continuous phase after emulsification was below detection limit.[11] In a second study, we were unable to determine the CNC shell thickness by SANS for an emulsion that was deliberately overloaded with CNC in the aqueous phase because the scattering of the 2-D interface superimposed with those of additional scattering of 3-D objects corresponding to the unadsorbed residual CNCs; the pure scattering of the interface was however recovered after removing the free CNCs by repeated washing.[12] For the CNC-II studied here, the fact that a pure power law of Q^{-2} scattering was obtained by SANS experiments on contrast-matched emulsions also demonstrates that there was no free CNC in the aqueous phase (see results section).

The average droplet diameters were measured by laser light scattering using a Horiba LA-960 particle size distribution analyzer (Kyoto, Japan). Refractive indices of 1.43 and 1.33 were used for hexadecane and water, respectively. The measurements were systematically carried out in duplicate. The diameter was expressed as surface mean diameter D(3,2) (the Sauter diameter).

For direct visualization of the nanocelluloses at a model oil-water interface, a polymerizable emulsion was prepared using styrene instead of hexadecane. Hexadecane and styrene have similar surface tension (27 mN m^{-1} and 32 mN m^{-1}, respectively) and we checked by optical microscopy that they produced stable emulsion with the similar average diameters. Styrene–AIBN mixtures (ratio 100:1 w/w) were mixed with nanocelluloses dispersed in 50 mM of NaCl aqueous solution. The emulsions were made via sonication and then polymerized at 65 °C without stirring for 48 hours. The resulting beads were washed by repeated centrifugation. The dried beads were sputtered with platinum and visualized with a scanning electron microscope (SEM) (JEOL 6400F).

Small Angle Neutron Scattering (SANS) experiments. SANS experiments were carried out at room temperature using the PA20 and PAXY diffractometers at the Laboratoire Léon Brillouin

(CEA/CNRS) in Saclay (France). Three configurations with wavelength / sample-to-detector distance combinations of 6 Å / 1.1 m, 6 Å/8 m, and 15 Å /17.5 m were used for PA20. These covered a Q range from 0.0006 to 0.44 Å^{-1}, where Q is the scattering vector ($Q = 4\pi \sin \theta / \lambda$, where θ is half the scattering angle and λ is the neutron wavelength). Four configurations (5 Å / 1 m, 5 Å / 3 m, 8.5 Å / 5 m and 15 Å / 6.7 m) were used for PAXY, which covered a Q range from 0.002 and 0.5 Å^{-1}. The emulsions were systematically freshly prepared and the cream layers loaded into quartz cells (Hellma) with path lengths of 1 or 2 mm. The azimuthally averaged spectra were corrected for solvent, cell and incoherent scattering, as well as for background noise. In this three-component system (CNCs, water and hexadecane), the neutron contrasts where chosen so that only the shell of the droplet at the water/ hexadecane interface is probed. In practice, the scattering length densities (SLD) of water and oil were matched using mixtures of hydrogenated and deuterated solvents, respectively 100% D$_2$O and a mixture of hexadecane/deuterated hexadecane at 6.4 vol % / 93.6 vol% (SLD$_{water}$ = SLD$_{hexadecane}$). A creaming process systematically occurred since the hexadecane density is lower than that of water, the precise emulsion volume in the beam could then not be controlled from one sample to another. The intensity is thus treated as relative. It gives an average over the whole sample illuminated by the neutron beam of the order of a π/4x7.6x7.6x1mm = 45 mm^3, owing to the collimation used (diameter aperture in front of the sample of 7.6 mm, thickness of sample vial 1 mm).

Molecular dynamics simulations

A simulation box with dimensions approximately 30 nm × 7.4 nm × 4.152 nm (X × Y × Z) which contains 537 heptadecane chains, 19132 water and one cellulose nanocrystal (CNC) was created to mimic the interface of Pickering emulsion as shown in Figure 5. The water phase had an initial thickness of about 21 nm and the alkane phase had a thickness of 9 nm in the X-direction. Three models with degree of polymerization of 8 glucosyl units (DP 8) containing 24 chains for CNC II and 18 chains for CNC I were initially placed close to the center of the water phase with the chain direction oriented along Z axis. By applying periodic boundary condition in all directions, the DP 8 CNC represents a CNC with infinite chain length. Regarding CNC-I, there is still a debate in the cellulose community, about the shape of the cross section for an 18-chains model. For comparison,

7

two models of native Iβ nanocrystals were taken for simulation; CNC-IA and CNC-IB that differ in shape of fibril cross-section. The former A-type exposes more hydrophilic surface, minimizing the hydrophobic surface (plane 1 0 0), while the latter (B-type) contains a larger hydrophobic surface (see the model cross sections in Figure S3). In order to overcome this uncertainty, we have built the two models for energy and entropy calculation and obtained consistent result.

Molecular dynamics (MD) simulations were carried out using GROMACS package, version 2021.1 combined with the GROMOS 56A$_{carbo}$ carbohydrate force field and SPC water model using NPT ensemble. Temperature and pressure were controlled at 300 K and 1 bar respectively. The total simulation last for 200~400 ns with frame saved every 20 ps. Entropy was estimated using the two-phase thermodynamic (2PT) model as used in previous work (Chen et al., 2017; Lombardo et al., 2018; Pascal, Lin, & Goddard III, 2011). All the parameters used are described in the Supplementary information.

RESULTS AND DISCUSSION

Characterization of cellulose nanocrystals

Table 1. Surface charge density (Sc), Zeta potential and dimensions of CNC-I and CNC-II.

Samples	SC	ζ-potential	Length(nm)		Width (nm)		Thickness (nm)	
	(mmol/g)	(mV)	SANS*	TEM	SANS*	TEM	SANS*	AFM
CNC-I	0.087 ± 0.03	- 42.3 ± 2.7	175 ± 25	118 ± 65	21 ± 1	7 ±3	6.5 ± 0.5	6.0 ±2.5
CNC-II	0.085 ± 0.01	- 41.9 ± 1.9	75 ± 25	65 ±22	22 ± 2	7 ±3	3.5 ± 0.5	3.4 ±1.5

* Average dimensions of CNC-I and CNC-II in dispersions at 2 mM NaCl determined from the SANS curve fit with the parallelepiped form factor

Native and mercerized CNCs were recovered from hydrolyzed native and mercerized MFCs respectively (Figure 1). Their characterization was carried out in the previous paper[23] and main values reported in Table 1. CNC-II are shorter and thinner than CNC-I, but with the same width. The apparent discrepancy between the size obtained by TEM and SANS for the width of both CNC-I and CNC-II comes from the fact the SANS gives an average width of CNCs that are composed of several crystallites while TEM images enabled to obtain the size of individualized crystallites. The respective widths of 21 nm measured by SANS and 7 nm by TEM, obtained for both types of CNC, corresponds thus to an average of 3 individual crystallites by lateral association, as previously reported for CNC-I.[3, 24, 26]
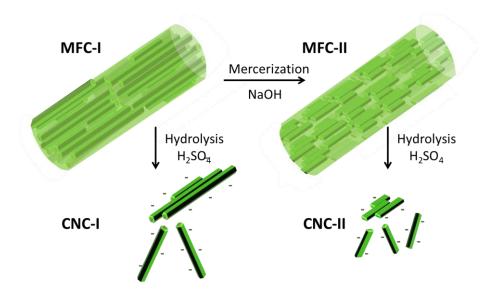

Figure 1. Schematic illustration of the cellulosic modification

Emulsion characterization and organization at the oil-water interface

Oil-in-water Pickering emulsions prepared at a 20/80 ratio were compared using CNC suspensions at concentrations between 0.8 and 3 g/L. Since all the CNCs are adsorbed at the interface (see experimental section), their amount can be directly expressed to the hexadecane volume, which corresponds to 7 to 27 mg of CNCs per mL of hexadecane.

For all the concentrations, a single peak in drop size distribution is obtained (curves in Figure S2). Figure 2 shows the average drop diameter (D[3,2]) as a function of the CNC concentration. The curves for CNC-I and CNC-II follow the same trends; below a m_p of 7 g/mL of hexadecane, which corresponds to suspensions at 1.4 g/L of CNC mixed at a ratio 80/20, the drop diameter decreases sharply with the CNC concentration, in accordance with the limited coalescence process[33] (Figure 2a).
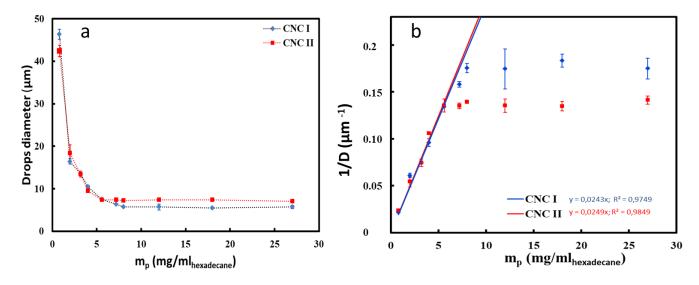

Figure 2. Evolution of (a) the average droplets diameter and (b) the coverage ratio for both types of CNC as a function of the mass of CNC per mL of hexadecane.

The limited coalescence process occurs only for irreversible adsorption of the particles and predicts a direct relationship between the amount of nanoparticles and the interfacial area. The droplet diameter is then controlled purely by the amount of CNCs since all the nanoparticles are adsorbed at the interface. This is better visualized when the inverse drop diameter 1/D is plotted against the amount of CNCs per mL of hexadecane (m_p) (Figure 2b). A linear dependence is obtained at low concentration with a slope depending on the surface coverage (C) and thickness of the interfacial layer (h) (equation 1).

$$\frac{1}{D} = \frac{m}{6\,C\,h\,\rho\,V_{oil}} = \frac{m_p}{6\,C\,h\,\rho}$$ (Equation 1)

And $\quad$ C = 1 / (6 x slope x 1.6 x h) (Equation 2)

10

Where ρ is the density (1.6 g/cm^3), m the mass of CNC and V_{oil} the volume of hexadecane included in the emulsion. Since the densities for CNC-I and CNC-II are almost identical, the slope at low concentration is linked to the coverage arrangement and/or the thickness variation.

At the lower concentrations, the same linear behavior is observed for both emulsions up to a critical concentration of around 5-7 mg/mL hexadecane. In this domain the drop coverage is constant, regardless of the amount of CNC, increasing CNC concentration leads to a larger interfacial area that allows stabilizing lower drop diameters as described elsewhere.[15] In the higher concentration domain, the deviation leads to a plateau value of the diameter (Figure 2). The average drop diameters stabilize to values around 5 µm for CNC-I and 7 µm for CNC-II. The slightly lower limit diameters obtained for CNC-I was not expected since CNC-II are smaller and thinner, and they should more easily organize and bend at the interface. It revealed that the adsorption capacity is slightly different for the two types of CNC. This different organization was not visible on SEM micrographs of polystyrene beads polymerized after coverage by CNC-I and CNC-II. Since these drops are dried for visualization, they tend to shrink and both show evenly distributed rod-like particles on the surface of the droplets, building a dense armored layer in both cases (Figure 3).
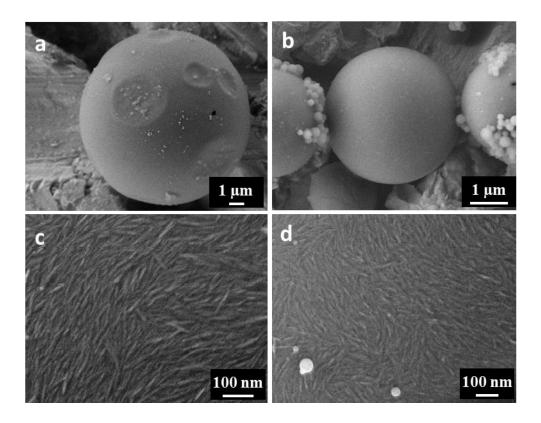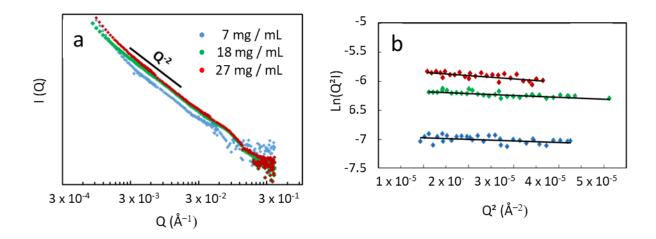
Figure 3. SEM images of polymerized styrene-in-water emulsions stabilized by CNC-I (a and c) and CNC-II (b and d)

The CNC-II-based emulsions were probed by SANS at three concentrations above the critical concentration, where the diameter variation is low. In this range, CNCs undergo surface densification, The result can be compared to the interface layer thickness of native CNC-I measured in a previous work[12]. In these conditions, only the shell contributes to the scattering (see experimental section) since the drop diameter (5 to 7 μm) is large compared to the typical spatial scale probed by the SANS ($D[3,2] \gg 1/Q_{min}$). As a result, the structural parameters of spherical hexadecane droplet (size and shape) do not influence the scattering in the Q-range window probed, the interface can thus be analyzed as a thin 2D flat film. Figure 4 shows the scattering intensity as a function of the scattering vector (Q) of the samples, displaying a power law decrease following Q^{-2} in the low Q range, which is characteristic of the scattering of two-dimensional objects. The form factor of the interface viewed as a film may be then modeled by a simple geometric model of a thin disc of thickness *2h* and a very large radius.[35][19]

Figure 4: SANS data. (a) the variation of intensity as a function of the scattering vector for three CNC concentrations and (b) the values in the low Q domain that allowed calculating the thickness of the interfacial layer according to equation 2.

The *h* value was then directly extracted from the slope of the curve $\ln(IQ^2)$ as a function of Q^2 (Figure 4b) according to equation 3 and reported in Table 2.

$$\ln(IQ^2) \approx \ln\left(\frac{2}{R^2}\right) - Q^2 \frac{h^2}{3} \qquad \text{(Equation 3)}$$

Table 2. Average thickness in nm of the layer of CNCs on the surface of the drops measured from SANS at different concentrations given in (g/L) for the CNC starting aqueous suspension and in (mg/mL hexadecane) for the CNC in the final emulsion. Values are taken from Cherhal et al.[12] for CNC-I and from the present work for CNC-II.

	Concentration of CNC in the aqueous phase (g/L)	Concentration of CNC, (mg/mL hexadecane)	Thickness of the interfacial layer (nm)
CNC-I	0.8	7	7 ±2
	2	18	7 ± 1

	5	45	7 ± 1
	0.8	7	9 ± 1
CNC-II	2	18	10 ± 1
	3	27	14 ± 1

According to equation 1 and using the shell thickness measured at the lowest concentration (7 nm for CNC-I and 9 nm for CNC-II), the coverage (C) at low concentration is 71% for CNC-I and 46% for CNC-II. The C value for CNC-II is however probably underestimated because the thickness value varies with concentration and we don't have the precise value for the low concentration range.

Increasing CNC concentration above 7 mg/mL hexadecane, the droplet diameter was constant regardless of the CNC concentration (Figure 2), while all CNCs are adsorbed at the interface.[12] This was confirmed by the fact that we always observe a Q^{-2} decay in SANS (see experimental section). The combination of a droplet diameter insensitive to particle concentration and the absence of particles in the bulk is rarely observed for Pickering emulsions. The critical concentration is generally associated with surface saturation and particles are released in the bulk. This is not the case in the present system for both CNCs, and explained by a reorganization of the nanorods leading to a higher 2D stacking density.[15] The anisotropy of the particles allows a reorientation of the rods which leads to an increase in the coverage rate at the droplet surface.

To evaluate the structure at the interface, the constant thickness of the interfacial layer of 7 nm for CNC-I regardless of the concentration matched perfectly with the thickness of the particle (Table 1). It suggested that individual CNC-I particles lie flat as a monolayer and are not adsorbed on the edge, otherwise the thickness would have been closer to their width (21 nm). On the contrary, for CNC-II stabilized emulsions, the thickness of the interfacial layer increases from 9 nm to 14 nm with increasing CNC-II concentration (Table 2). This shell thickness is far from the thickness of individual particle (3.5 nm) and close to the width of the CNC-II (22 nm). This is induced by the way the crystals

adsorb at the interface, it indicates that, unlike CNC-I, CNC-II is either adsorbed on the edge or forms multilayers on the surface.

The potential multilayer formation was investigated forcing aggregative conditions. This was measured in bulk water as a function of ionic strength concentration (see Figure S1). CNC-I and CNC-II showed identical aggregation behavior, making the probability of a multilayer unlikely.

Finally, it was observed that both crystal types irreversibly adsorbed at the interface, but organized differently on the drop surface, which might be related to the high orthotropic character of the cellulose II crystals obtained by mercerization.[27] It was observed that CNC-I is firmly adsorbed with a constant thickness on a large surface area and at higher concentration a densification occurs by reorientation of the nanocrystals at the interface. For CNCs-II the thickness varies, they might not lay flat on the surface but on an edge that leads to an increase in the apparent layer thickness when increasing the amount of CNCs at the interface, giving the possibility to tilt at a different angle in addition to the 2D packing.

MD Simulation of CNC-I and CNC-II models in regard to interfacial adsorption

This assumption was reproduced in MD simulation (Figure 5). Both CNC-I and CNC-II models were initially placed in the middle of the water phase and allowed to move to minimize the system. Both CNC-I and CNC-II adsorbed onto the heptadecane/water interface and they both oriented their hydrophobic surfaces (0 1 0 & 1 0 0, respectively) to the interface, and maintained this orientation throughout the remainder of the simulation showing a preferential plane. The main difference between the two allomorphs is that CNC-I partially penetrated the alkane phase, whereas the CNC-II was fully immersed in the water phase. The effective cross-section of the native CNC (Iβ form) cannot be assessed with certainty with respect to the crystallographic plane for the current sample, therefore we compared two potential models of CNC I, one minimizing the exposure of hydrophobic surface (CNC-IA) and the other, the generally used model, exposing more hydrophobic surface (CNC-IB) (see

Figure S3). With CNC-IA, despite the low hydrophobicity, CNC-I oriented and maintained the (1 0 0)

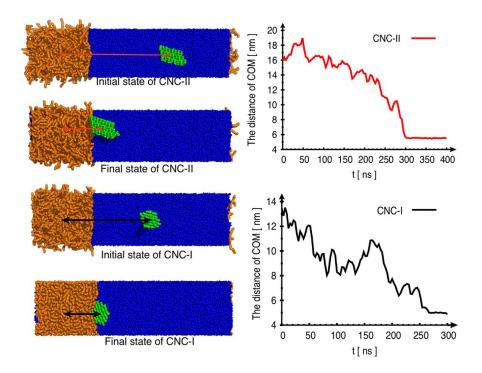hydrophobic surface to the interface, like for CNC-IB (Figure S4).

Figure 5: Snapshot of the sorption simulation of CNC (II and IB) onto the alkane/water interphase and

center of mass distance between CNC and alkane phase.

Table 3: Difference free energy and its components between CNC-I and CNC II adsorbed and

unabsorbed surfaces Two potential models of CNC I were investigated one minimizing the exposure

of hydrophobic surface (CNC-IA) and the other one most often used more hydrophobic (CNC-IB).

	CNC-IA	CNC-IB	CNC-II
$\Delta G = \Delta H - T\Delta S$ (mJ/m^2)	-26 (±7)	-53 (±7)	-55 (±12)
$\Delta H = H_{Final} - H_{initial}$ (mJ/m^2)	-21 (±2)	-41 (±2)	-36 (±3)
$-T\Delta S = -T(S_{final} - S_{intial})$ (mJ/m^2)	-5 (±10)	-12 (±10)	-19 (±17)

The free energy variation of adsorption was calculated as the sum of variation of total enthalpy and

entropy. Since the number of water molecules is much larger than that of the alkane molecules, the

entropy of the system is dominated by the water entropy. As shown in Table 3, the Gibbs free energy variation that drives the adsorption of CNC from bulk water to alkane/water interface is -55 mJ/m^2 for allomorph II and -53 mJ/m^2 for allomorph IB (the frequently used model), indicating that the adsorption is a spontaneous thermodynamic process, and that the adsorption should be highly stable. Even considering the crystal model minimizing the exposure of hydrophobic surface (CNC-IA), the value is lower but still negative giving the same tendency. Energy decomposition shows that both enthalpy and entropy contribute to the decreasing free energy, but the contribution of enthalpy is about 2~3 fold than that of entropy. This means that the adsorption would depend little on temperature.

In this study, the entropy gain is essentially due to the exclusion of water from cellulose and alkane surface upon adsorption. As shown in the entropy gradient profile in Figure S5, water gains entropy when being expelled from cellulose surface to bulk, but loses entropy when being expelled from alkane surface into bulk. However, the net contribution leads to a gain in entropy.
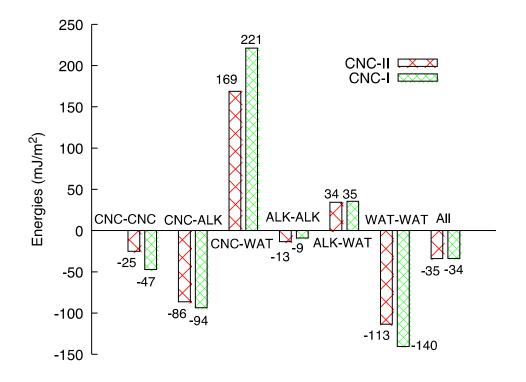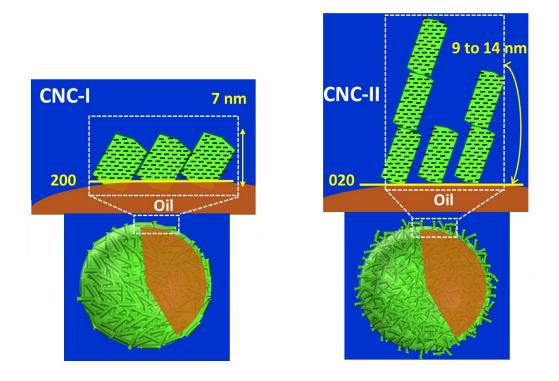

Figure 6: Energy decomposition analysis for the energy difference between final (adsorbed) and initial (desorbed) states. (CNC=glucose, ALK=alcane, WAT=water)

This simulation also illustrates the preferred crystallographic plane of CNC that interacts with the interface. If the adsorption was not specific to the nature of the interface, the particle should adsorb by the larger and flatter surface that gives better contact area (and thus expel more water from the interface gaining more solvent entropy). However, for both CNCs it was the hydrophobic crystalline plane that is the smaller one that went in contact with the alkane. The variation of water–alkane enthalpy due to the removal of water at the interface (ALK-WAT) is around $+35$ mJ/m^2 which is compensated by about -90 mJ/m^2 of the glucose-alkane (CNC-ALK) as shown in Figure 6, leading to the spontaneous adsorption of the particles at the interface. This is in line with a recent article (Kishani et al. J Coll & int Sci 2021) using MD to calculate thermodynamic parameters of XG adsorption on the crystalline surfaces of the CNC. It validates that the CNCs adsorb spontaneously to the interface through the hydrophobic plan despite its very low surface of exposition; that is plan (1 0 0) for CNC-I even when its surface is minimized and (0 1 0) for CNC-II, and this adsorption is driven both by entropy and enthalpy.

Figure 7: A schematic representation of both allomorphs firmly adhering at the hexadecane surface. Increasing the concentration, CNC-I (left) align at the interface covering the interface, at constant

thickness. On the other hand, CNC-II (right) adsorb onto the hexadecane only by a small face with the major volume fraction in the water phase. The particles are then inclined at low concentration but stand upright upon densification.

CONCLUSION

Both CNC-I and CNC-II adsorb irreversibly at the hexadecane /water interface, producing highly stable Pickering emulsions. CNC-I leads to a 7 nm thick layer regardless of CNC concentration. Thus, increasing the concentration led to a densification of the interfacial layer due to the 2D re-orientation of the rods at the interface leading to the increased coverage. For CNC-II, the crystal is thinner (3.5 nm) but the measured thickness of the interfacial layer was larger than that of CNC-I. Furthermore, the increase in CNC-II concentration was accompanied by an increase of the interface thickness from 9 to 14 nm, which can be explained by adsorption on the hydrophobic edge of the CNC-II particles as schematically proposed in Figure 7. Molecular dynamic simulation of the different types of cellulose crystals showed that they both spontaneously adsorbed to the interface driven both by entropy and enthalpy. However, the contribution is mainly due to enthalpy since the variation of is about 2~3 fold that of entropy. Thus, crystalline planes parallel to the pyranose plane, (1 0 0) and (0 1 0) for CNC-I and CNC-II respectively, preferentially adsorb at the interface, leading to a face-on adsorption for CNC-I, and an edge-on adsorption in the case of CNC-II. As a result, CNC-I forms a flat and uniform interfacial layer, while CNC-II forms a rougher layer with adjustable thickness, providing new insight into the affinity and arrangement of cellulose I and cellulose II at an interface.

SUPPORTING INFORMATION

Details on the molecular dynamics simulations and extra figures: entropy gradient of water and snapshots of the cross-section. Drop diameter distribution of emulsions. I = f(Q) SANS curves of CNC suspensions for their aggregation with increasing ionic strength.

AUTHOR CONTRIBUTIONS

The manuscript was written through contributions of all authors. All authors have given approval to the final version of the manuscript.

FUNDING SOURCES

REFERENCES

1.   Nishiyama, Y., Structure and properties of the cellulose microfibril. *J. Wood Sci.* **2009,** 55, (4), 241-249.

2.   Carpita, N. C.; Gibeaut, D. M., Structural models of primary-cell walls in flowering plants - Consistency of molecular-structure with the physical-properties of the walls during growth. *Plant J.* **1993,** 3, (1), 1-30.

3.   Elazzouzi-Hafraoui, S.; Nishiyama, Y.; Putaux, J. L.; Heux, L.; Dubreuil, F.; Rochas, C., The shape and size distribution of crystalline nanoparticles prepared by acid hydrolysis of native cellulose. *Biomacromolecules* **2008,** 9, (1), 57-65.

4.   Nishiyama, Y.; Langan, P.; Chanzy, H., Crystal structure and hydrogen-bonding system in cellulose 1 beta from synchrotron X-ray and neutron fiber diffraction. *JACS* **2002,** 124, (31), 9074-9082.

5.   Okano, T.; Sarko, A., Mercerization of cellulose. 2 Alkali cellulose intermediates and a possible mercerization mechanism. *J. Appl. Polym. Sci.* **1985,** 30, (1), 325-332.

6.   Lehtio, J.; Sugiyama, J.; Gustavsson, M.; Fransson, L.; Linder, M.; Teeri, T. T., The binding specificity and affinity determinants of family 1 and family 3 cellulose binding modules. *Proc. Natl. Acad. Sci. U. S. A.* **2003,** 100, (2), 484-489.

7.   Oza, K. P.; S.G., F., Multiple emulsions stabilized by colloidal microcrystalline cellulose. *J. Dispersion Sci. Technol.* **1989,** 10, (2), 163-185.

8.   Ramsden, W., Separation of solids in the surface-layers of solutions and "suspensions" (observations on surface-membranes, bubles, emulsions and mechanical coagulation). *Proc. Roy. Soc.* **1903,** 72, 156-164.

9.   Pickering, S. U., Emulsions. *Journal of Chemical society* **1907,** 91, 2001-2021.

10.   Kalashnikova, I.; Bizot, H.; Cathala, B.; Capron, I., New Pickering Emulsions Stabilized by Bacterial Cellulose Nanocrystals. *Langmuir* **2011,** 27, (12), 7471-7479.

11.   Kalashnikova, I.; Bizot, H.; Cathala, B.; Capron, I., Modulation of Cellulose Nanocrystals Amphiphilic Properties to Stabilize Oil/Water Interface. *Biomacromolecules* **2012,** 13, (1), 267-275.

12.   Cherhal, F.; Cousin, F.; Capron, I., Structural Description of the Interface of Pickering Emulsions Stabilized by Cellulose Nanocrystals. *Biomacromolecules* **2016,** 17, (2), 496-502.

13.   Capron, I.; Rojas, O. J.; Bordes, R., Behavior of nanocelluloses at interfaces. *Curr. Opin. Colloid Interface Sci.* **2017,** 29, 83-95.

14.   Zhai, X.; Lin, D.; Liu, D.; Yang, X., Emulsions stabilized by nanofibers from bacterial cellulose: New potential food-grade Pickering emulsions. *Food Res. Int.* **2018,** 103, 12-20.

15.   Capron, I., *Application of Nanocellulose as Pickering Emulsifier*. Nanocellulose Sustain. (2018), pp. 175-196.

16.   Saelices, C. J.; Capron, I., Design of Pickering Micro- and Nanoemulsions Based on the Structural Characteristics of Nanocelluloses. *Biomacromolecules* **2018,** 19, (2), 460-469.

17.   Revol, J. F.; Dietrich, A.; Goring, D. A. I., Effect of mercerization on the crystallite size and crystallinity index in cellulose from different sources. *Can. J. Chem.* **1987,** 65, (8), 1724-1725.

18.   Neto, W. P. F.; Putaux, J. L.; Mariano, M.; Ogawa, Y.; Otaguro, H.; Pasquini, D.; Dufresne, A., Comprehensive morphological and structural investigation of cellulose I and II nanocrystals prepared by sulphuric acid hydrolysis. *RSC Adv.* **2016,** 6, (79), 76017-76027.

19.   Li, X.; Li, J.; Gong, J.; Kuang, Y. S.; Mo, L. H.; Song, T., Cellulose nanocrystals (CNCs) with different crystalline allomorph for oil in water Pickering emulsions. *Carbohydr. Polym.* **2018,** 183, 303-310.

20.   Haouache, S.; Jimenez-Saelices, C.; Cousin, F.; Falourd, X.; Pontoire, B.; Cahier, K.; Jerome, F.; Capron, I., Cellulose nanocrystals from native and mercerized cotton. *Cellulose* **2022,** 29, (3), 1567-1581.

21.   Lin, F. B.; Pignon, F.; Putaux, J. L.; Jean, B., Temperature-triggered formation of a cellulose II nanocrystal network through regioselective derivatization. *Nanoscale* **2021,** 13, (13), 6447-6460.

22.   Revol, J. F.; Bradford, H.; Giasson, J.; Marchessault, R. H.; Gray, D. G., Helicoidal self-ordering of cellulose microfibrils in aqueous suspension. *Int. J. Biol. Macromol.* **1992,** 14, (3), 170-172.

23.   Haouache, S.; Jimenez-Saelices, C.; Cousin, F.; Falourd, X.; Pontoire, B.; Cahier, K.; Jérome, F.; Capron, I., Cellulose nanocrystals from native and mercerized cotton. *Cellulose* **2022**, 29 (3) , 1567-1581.

24.   Cherhal, F.; Cousin, F.; Capron, I., Influence of charge density and ionic strength on the aggregation process of cellulose nanocrystals in aqueous suspension, as revealed by small-angle neutron scattering. *Langmuir* **2015,** 31, (20), 5596-5602.

25.   Peddireddy, K. R.; Capron, I.; Nicolai, T.; Benyahia, L., Gelation Kinetics and Network Structure of Cellulose Nanocrystals in Aqueous Solution. *Biomacromolecules* **2016,** 17, (10), 3298-3304.

26.   Cherhal, F.; Cathala, B.; Capron, I., Surface charge density variation to promote structural orientation of cellulose nanocrystals. *Nord. Pulp Pap. Res. J.* **2015,** 30, (2), 126-131.

27.   Yamane, C.; Hirase, R.; Miyamoto, H.; Kuwamoto, S.; Yuguchi, Y., Mechanism of structure formation and dissolution of regenerated cellulose from cellulose/aqueous sodium hydroxide solution and formation of molecular sheets deduced from the mechanism. *Cellulose* **2015,** 22, (5), 2971-2982.

FOR TABLE OF CONTENTS USE ONLY

TITLE: EDGE-ON (CELLULOSE II) AND FACE-ON (CELLULOSE I) ADSORPTION OF CELLULOSE NANOCRYSTALS AT THE OIL/WATER INTERFACE; A COMBINED ENTROPIC AND ENTHALPIC PROCESS.

AUTHORS : SOMIA HAOUACHE[1,2,#], YU CHEN[3,#], CLARA JIMENEZ[1], FABRICE COUSIN[4], PAN CHEN[3], YOSHIHARU NISHIYAMA[5], FRANÇOIS JEROME[2], ISABELLE CAPRON[1]